Geophysical Research Letters

RESEARCH LETTER
10.1029/2024GL109116

Dynamic Component of the Asthenosphere: Lateral Viscosity Variations Due To Dislocation Creep at the Base of Oceanic Plates

V. Patočka[1], H. Čížková[1], and J. Pokorný[1]

[1]Faculty of Mathematics and Physics, Department of Geophysics, Charles University, Prague, Czech Republic

Key Points:

- Substantial component of asthenospheric weakening is dynamic, caused by dislocation creep at the base of tectonic plates
- Dynamic weakening scales with the surface velocity both below the subducting and the overriding plate
- The resulting scaling law is employed in an apriori estimate of the lateral viscosity variations below Earth's oceans

Supporting Information:

Supporting Information may be found in the online version of this article.

Correspondence to:

V. Patočka,
vojtech.patocka@matfyz.cuni.cz

Citation:

Patočka, V., Čížková, H., & Pokorný, J. (2024). Dynamic component of the asthenosphere: Lateral viscosity variations due to dislocation creep at the base of oceanic plates. *Geophysical Research Letters*, *51*, e2024GL109116. https://doi.org/10.1029/2024GL109116

Received 6 MAR 2024
Accepted 1 JUN 2024

Author Contributions:

Conceptualization: V. Patočka, H. Čížková
Data curation: V. Patočka
Formal analysis: V. Patočka
Investigation: V. Patočka, H. Čížková, J. Pokorný
Methodology: V. Patočka
Visualization: V. Patočka, H. Čížková, J. Pokorný
Writing – original draft: V. Patočka
Writing – review & editing: H. Čížková, J. Pokorný

Abstract The asthenosphere is commonly defined as an upper mantle zone with low velocities and high attenuation of seismic waves, and high electrical conductivity. These observations are usually explained by the presence of partial melt, or by a sharp contrast in the water content of the upper mantle. Low viscosity asthenosphere is an essential ingredient of functioning plate tectonics. We argue that a substantial component of asthenospheric weakening is dynamic, caused by dislocation creep at the base of tectonic plates. Numerical simulations of subduction show that dynamic weakening scales with the surface velocity both below the subducting and the overriding plate, and that the viscosity decrease reaches up to two orders of magnitude. The resulting scaling law is employed in an apriori estimate of the lateral viscosity variations (LVV) below Earth's oceans. The obtained LVV help in explaining some of the long-standing as well as recent problems in mantle viscosity inversions.

Plain Language Summary The motion of lithospheric plates at the Earth's surface is enabled by a weak underlying layer—the asthenosphere. The origin of this low viscosity layer is still subject of discussion. Presence of water or partial melt were proposed as possible reasons of its reduced viscosity. Another mechanism that may lead to weakening is non-linear deformation. Rheological description of asthenospheric material includes dislocation creep, a deformation mechanism that depends on the velocity contrast between the lithospheric plate and underlying mantle—the faster the plates are, the weaker the underlying layer becomes and vice versa. Here we argue that a substantial component of asthenospheric weakening is dynamic, caused by this deformation mechanism. We evaluate numerical models of subduction including dislocation creep and derive a relation between the surface velocity of oceanic plates and the magnitude of the underlying asthenospheric viscosity. This allows us to estimate how the viscosity varies under different oceanic plates on Earth, which is otherwise hard to constrain. Our results indicate that the asthenosphere below the Pacific plate should be particularly weak.

1. Introduction

Defined as a mechanically weak layer that accommodates vertical isostatic movements of Earth's continents, the asthenosphere is originally a geodynamic concept (Barrell, 1914). Later, it was attributed with low velocities and high attenuation of seismic waves (e.g., Dziewonski & Anderson, 1981; Montagner & Tanimoto, 1991), and also with high electrical conductivity (Shankland et al., 1981)—observations typical for the presence of melt, leading to speculations about widespread partial melting in the upper mantle (e.g., Hirschmann, 2010; Lambert & Wyllie, 1970; Mierdel et al., 2007; Shankland et al., 1981). Recently, Hua et al. (2023) showed that the onset of partial melting is visible in receiver function data from globally distributed seismic stations. S.-I. Karato (2012), however, argues that the origin of the asthenosphere lies elsewhere. He explains the geophysical observations by assuming a sharp change in the water content of the suboceanic mantle. Due to the second-stage partial melting, ascending mantle material becomes dehydrated approximately 70 km below mid-ocean ridges (J. Morgan & Morgan, 1999), at the same depth at which the 5%–10% drop in seismic velocity is observed in old oceanic plates (e.g., Kawakatsu et al., 2009; Rychert & Shearer, 2009), but where geothermal models predict subsolidus temperatures (i.e., where a sharp contrast in the melt content is unlikely, Figure 5 in S.-I. Karato, 2012).

A third hypothesis, pursued for example by J. P. Morgan et al. (2013), is that the asthenosphere is a region where plumes hotter than the average mantle spread below the lithosphere, forming a global pool of elevated temperatures with a negative thermal gradient at its base explaining the gradual increase of seismic velocities at ~250–350 km depth (Cammarano et al., 2009).

The above three hypotheses of asthenospheric origin are not necessarily contradictory, because they focus on different geophysical observations: (a) The lithosphere-asthenosphere boundary (LAB), indicated in the oceanic plates at the depths ∼70 km by the drop in wavespeed, could be related to a change in the water content, (b) The receiver-function data at ∼150 km depth (Hua et al., 2023) could be sensitive to a widespread onset of the first-stage, low degree partial melting, (c) The yet deeper increase of seismic velocities at ∼250–350 km depth could be linked with a negative thermal gradient resulting from accumulation of hot material from mantle plumes in the sublithospheric region.

Geodynamic significance of the asthenosphere, that is, that on geological timescales, is in transferring stresses to/from tectonic plates (Coltice et al., 2019; Forsyth & Uyeda, 1975). The lateral extent of some of the major tectonic plates largely exceeds the depth of the mantle, indicating a long-wavelength mantle convection flow (Su & Dziewonski, 1992; Hager & Richards, 1989; M. Richards & Engebretson, 1992). Such a large aspect ratio cells are, however, theoretically unstable at Earth's Rayleigh number (F. H. Busse, 1985; Turcotte & Schubert, 1982)—a viscosity contrast between the asthenosphere and the underlying mantle is required in order to stabilize these long-wavelength structures (Bunge et al., 1996; Ahmed & Lenardic, 2010; F. Busse et al., 2006; Lenardic et al., 2006).

Lenardic et al. (2019) argue that plate tectonics is a self-sustaining system whose components: the asthenosphere, subducting slabs, and long-wavelength flow are mutually interdependent. Subduction of large tectonic plates generates an asymmetry between the convective velocity of down- and up-flows, which in turn results in a sub-adiabatic thermal gradient in Earth's mantle (F. H. Busse, 1985; Jeanloz & Morris, 1987). This, together with the pressure dependence of viscosity, increases the viscosity contrast between the upper and the lower mantle—a necessary ingredient for channelization of horizontal mantle flow and thus for reducing the otherwise destabilizing horizontal drag at the base of large tectonic plates. The system of feedbacks and loops is analyzed in a number of studies (see references in Lenardic et al., 2019) and many of them neglect dislocation creep in the mantle.

All the above studies argue that the asthenosphere is of thermal and/or compositional origin. Here we explore sublithospheric weakening due to dislocation creep at the base of subducting plates, activated by the high strain-rates that result from the relative motion of oceanic plates and the underlying mantle (dynamically generated asthenosphere).

The idea that dislocation creep is important in the shallow mantle is not new. In fact, until the 90s dislocation creep was thought to dominate over diffusion creep throughout the entire upper mantle (e.g., Carter & Ave'-Lallemant, 1970; Green & Radcliffe, 1972). S. Karato and Wu (1993) then argued that dislocation creep is localized only in the asthenosphere while the cold and shallow and the deeper mantle deform via diffusion creep. Dislocation creep is also the main candidate for generating a lattice preferred orientation in minerals and is thus commonly used in interpreting seismic anisotropy, which is strongest near athenospheric depths (e.g., Becker et al., 2014; Debayle et al., 2005; Walpole et al., 2017).

In geodynamic modeling on a regional scale, dislocation creep is a typical ingredient, promoting strain-rates in regions of high stresses, enhancing velocities (van den Berg et al., 1993), facilitating motion of the stiff subducting plates (e.g., Bessat et al., 2020; Billen & Hirth, 2007; Cerpa et al., 2022; Chertova et al., 2012; Garel et al., 2014; Pokorný et al., 2021; Yang et al., 2018) and reducing the trench retreat rate (Holt & Becker, 2016). In global numerical models, the effects of dislocation creep on the viscosity below tectonic plates were evaluated by Becker (2006) and Stadler et al. (2010), but no one, to our knowledge, has related asthenospheric weakness to the surface velocities of tectonic plates and explored the implications of such a relation. Dynamic asthenosphere is considered in the works of A. G. Semple and Lenardic (2018); A. Semple and Lenardic (2020); A. G. Semple and Lenardic (2021), but their numerical models employ an idealized, layered viscosity structure with activation parameters smaller compared to the experimental values. Moreover, the asthenospheric viscosity reduction is quantified only in the last of these works (A. G. Semple & Lenardic, 2021), where a conceptually different, stagnant lid model is investigated, in which weakening is a result of high strain-rates in a convecting layer below an immobile lithosphere (similarly in Schulz et al., 2020).

Mantle viscosity is a key to understanding fundamental Earth science questions and numerous studies attempted to infer it from a wide variety of data. Primary constraints were obtained from the inversions of Earth's geoid (e.g., Hager et al., 1985; Hager & Richards, 1989; Ricard et al., 1993) and postglacial rebound (e.g., Mitrovica &

Forte, 2004; Peltier, 1998), and from laboratory experiments of pressurized rocks (e.g., S.-I. Karato, 2008). Most studies have considered only radially dependent (i.e., 1D) viscosity structure, and yet wide-ranging estimates of viscosity profiles have been obtained. M. A. Richards and Lenardic (2018) noted that the mismatch in the astenosphere might be caused by the fact that the long-wavelength geoid and postglacial rebound are both sensitive to a combination of the viscosity contrast between the asthenosphere and underlying mantle and the asthenospheric thickness (Cathles parameter) rather than to the actual value of viscosity in the asthenosphere.

After inversions aiming at the radial viscosity structure, efforts have been invested in inferring also the lateral viscosity variations (LVV) in some parts of the mantle, especially the asthenosphere. Čadek and Fleitout (2003) have demonstrated that the viscosity below the oceanic plates is by two orders of magnitude weaker than the deep continental roots. Yang and Gurnis (2016) and Mao and Zhong (2021) assume weak plate margins in their inversions, but do not consider dislocation creep at the base of tectonic plates. Yang and Gurnis (2016) include high-accuracy residual topography measurements into the fitted data and obtain asthenospheric LVV much smaller than those predicted by forward models with laboratory-based activation parameters of diffusion creep—suggesting that some weakening mechanism is missing around the cold and stiff subducting slabs in their models. Mao and Zhong (2021) use weak plate margins in their convection model to obtain surface velocities consistent with the present-day plate motions. In order to match the toroidal component of the surface velocity field, they need to prescribe that the circum-pacific margin is considerably less resistant than other plate margins, but a physical reason for such an ad-hoc manipulation is not clear.

Subduction controls the distribution and fragmentation of Earth's tectonic plates (Mallard et al., 2016). Slab dynamics are therefore an important and somewhat independent indicator of the mantle viscosity structure. In the past, subduction models have been used to infer the upper to lower mantle viscosity ratio (Liu et al., 2021; Čížková et al., 2012). Here we estimate the laterally dependent, that is, horizontally varying contribution of dislocation creep to sublithospheric weakening, without arguing against thermal and/or compositional effects—the different weakening mechanisms are likely superimposed in the real Earth. We assume that the dynamic weakening stems from the shear of mobile tectonic plates with respect to the underlying mantle. Slab pull on the subducted part of the lithospheric plates drives plate motion which in turn reinforces asthenospheric weakening in a dynamic feedback through nonlinear dislocation creep. We employ numerical models of subduction that include diffusion and dislocation creep with laboratory based parameters (Hirth & Kohlstedt, 2003), and study the relation between plate velocity and asthenospheric weakening. By comparing this relation with the current plate motions, we finally estimate dynamically generated weakening and the resulting LVV in the asthenosphere, improving the apriori information on the distribution of viscosity in Earth's mantle.

2. Subduction Models

We perform two families of "generic" subduction models, meaning that the initial and boundary conditions are not tailored to any specific geographic location. The governing equations are solved in an extended Boussinesq approximation in a 2D Cartesian box (Čížková et al., 2007) using a finite element package SEPRAN (Segal & Praagman, 2005). Mesh resolution is varying across the model domain, maximum of 2.5 km is around the crust-lithosphere boundary and 8 km is the resolution in the transition zone as well as the vertical resolution of the upper mantle (for a resolution test, see Supporting Information S1). Rheological description of the mantle and lithosphere is taken from Čížková and Bina (2013). Model parameters are listed in Table 1. In one family of models, the overriding plate is attached to the right boundary, mimicking Earth's regions with stationary trench and little to no motion of the overriding plate. In these models, denoted as "fixed OP", the trench rollback does not occur. In the second family of models, labeled as "mobile OP", a mid ocean ridge is imposed at the right top boundary. In this setup OP is free to move trenchwards and thus can accommodate trench rollback. We note that OP is strong and does not allow for horizontal extension, therefore rollback of the SP is associated with the motion of OP as a whole.

Within each family of models, the individual simulations differ by the initial age of the SP, ranging from 50 to 150 Myr at the trench (see Table 1 and Figure S3 in Supporting Information S1 illustrating the slab morphologies). Subduction evolution is evaluated in an extended Boussinesq model that includes buoyancy and latent heat effects of major mantle phase transitions at 410 and 660 km depths (e.g., Pokorný et al., 2023). A composite rheological model combines diffusion creep, dislocation creep and power-law stress limiter. An effective viscosity of the upper mantle and transition zone is calculated as

Table 1
Model Parameters

Symbol	Meaning	Value	Units
Upper mantle and oceanic lithosphere rheology			
A_{diff}	Pre-exponential parameter of diffusion creep[a]	1×10^{-9}	$Pa^{-1}\ s^{-1}$
A_{disl}	Pre-exponential parameter of dislocation creep[a]	31.5×10^{-18}	$Pa^{-n}\ s^{-1}$
E_{diff}	Activation energy of diffusion creep[a]	3.35×10^{5}	$J\ mol^{-1}$
E_{disl}	Activation energy of dislocation creep[a]	4.8×10^{5}	$J\ mol^{-1}$
V_{diff}	Activation volume of diffusion creep[a]	4.0×10^{-6}	$m^3\ mol^{-1}$
V_{disl}	Activation volume of dislocation creep[a]	11×10^{-6}	$m^3\ mol^{-1}$
n	dislocation creep exponent	3.5	–
D_y	Reference strain rate	1×10^{-15}	s^{-1}
σ_y	Stress limit	2×10^{8}	Pa
n_y	Stress limit exponent	10	–
R	Gas constant	8.314	$J\ K^{-1}\ mol^{-1}$
Lower mantle rheology			
A_{diff}	Pre-exponential parameter of diffusion creep	1.3×10^{-16}	$Pa^{-1}\ s^{-1}$
E_{diff}	Activation energy of diffusion creep[b]	2×10^{5}	$J\ mol^{-1}$
V_{diff}	Activation volume of diffusion creep[b]	1.1×10^{-6}	$m^3\ mol^{-1}$
Other model parameters			
L, H	Model domain dimensions (length, depth)	10^4, $2 \cdot 10^3$	Km
η_{crust}	Viscosity of the crust	10^{20}	Pa s
κ	Thermal diffusivity	10^{-6}	$m^2\ s^{-1}$
g	Gravitational acceleration	9.8	$m^2\ s^{-2}$
ρ_0	Reference density	3,416	$kg\ m^{-3}$
c_p	Specific heat	1,250	$J\ kg^{-1}\ K^{-1}$
α_0	Surface thermal expansivity	3×10^{-5}	K^{-1}
γ_{410}	Clapeyron slope of 410 km phase transition[c]	2×10^{6}	$Pa\ K^{-1}$
γ_{660}	Clapeyron slope of 660 km phase transition[c]	-2.5×10^{6}	$Pa\ K^{-1}$
$\delta_{\rho 410}$	Density contrast of 410 km phase transition[d]	273	$kg\ m^{-3}$
$\delta_{\rho 660}$	Density contrast of 660 km phase transition[d]	341	$kg\ m^{-3}$

Description of different models

Label	Initial age of SP (Myr)	Initial age of OP (Myr)	Ridge in the right top corner
M1	50	100	No (fixed OP)
M2	100	100	No (fixed OP)
M3	150	100	No (fixed OP)
M4	50	100	Yes (mobile OP)
M5	100	100	Yes (mobile OP)
M6	150	100	Yes (mobile OP)
M7	100	50	Yes (mobile OP)
M8	100	150	Yes (mobile OP)
M9	150	150	Yes (mobile OP)

[a]Parameters of wet olivine based on Hirth and Kohlstedt (2003). [b]Čížková et al. (2012). [c]Bina and Helffrich (1994). [d]Steinbach and Yuen (1995).

$$\eta_{\text{eff}} = \left(\frac{1}{\eta_{\text{diff}}} + \frac{1}{\eta_{\text{disl}}} + \frac{1}{\eta_y}\right)^{-1}. \quad (1)$$

The viscosity of diffusion creep is evaluated as

$$\eta_{\text{diff}} = A_{\text{diff}}^{-1} \exp\left(\frac{E_{\text{diff}} + pV_{\text{diff}}}{RT}\right), \quad (2)$$

where A_{diff} is pre-exponential parameter, E_{diff} is activation energy, p is lithostatic pressure, V_{diff} is activation volume of diffusion creep, R is the gas constant and T is temperature. Dislocation creep viscosity is

$$\eta_{\text{disl}} = A_{\text{disl}}^{-1/n} D^{(1-n)/n} \exp\left(\frac{E_{\text{disl}} + pV_{\text{disl}}}{nRT}\right), \quad (3)$$

where A_{disl}, E_{disl} and V_{disl} are the pre-exponential parameter, activation energy, and activation volume of dislocation creep, D is the second invariant of the total strain rate tensor, and the exponent $n = 3.5$ (Kameyama et al., 1999). Finally the power-law stress limiter viscosity is

$$\eta_y = \sigma_y D_y^{-(1/n_y)} D^{(1/n_y)-1} \quad (4)$$

where D_y is the reference strainrate, σ_y is the yield stress and the power-law exponent is taken as $n_y = 10$.

Activation parameters based on experimental data for wet olivine are assumed in the upper mantle and the transition zone (Hirth & Kohlstedt, 2003). We note that our activation energy of dislocation creep is in the range indicated also by van Hunen et al. (2005) to fit the seismically inferred thermal structure of the Pacific lithosphere. In the lower mantle we assume diffusion creep with parameters based on Čížková et al. (2012). Duration of each simulation is 100 Myr.

3. Dynamic Weakening Below the Subducting and Overriding Plates

In both model families, a distinct region forms below the SP, where the viscosity of dislocation creep is smaller than that of diffusion creep. We denote this compact, sub-plate domain where $\eta_{\text{disl}} < \eta_{\text{diff}}$ as the "dynamic asthenosphere" (or simply the asthenosphere in the following text). We define the dynamic weakening w as a positive number,

$$w(x,t) = \max\left(\log_{10}\frac{\min(\eta_{\text{diff}})}{\min(\eta_{\text{disl}})}, 0\right), \quad (5)$$

where the minima are taken over the region where $\eta_{\text{disl}} < \eta_{\text{diff}}$ (see Figure 1b). The quantity w is a measure of the viscosity reduction that is caused by the high strain-rate below the plate (or by the high stress—note that dislocation creep viscosity can be formulated either as a function of strain-rate or as a function of stress, see van den Berg et al., 1993). At each time t for each horizontal position x, the minima in Equation 5 are evaluated. In Figure 1d, we show how w is distributed both horizontally and temporarily in model M4.

The value of w is approximately constant up to $x \approx 0.8\, x_{\text{T}}$, where x_{T} is the time varying position of the trench. In subsequent analysis, we will represent the dynamic weakening below SP with the value of w averaged over $x \in (0.05, 0.8)\, x_{\text{T}}$ to avoid regions near the plate boundaries (ridge and trench) which are dominated by vertical flow (discussion of the near-trench region follows at the end of this section).

As the subducting slab starts sinking into the mantle, its velocity v_{SP} varies due to the increasing slab pull, varying resistance of the mantle and petrological buoyancy associated with the phase transitions (Figure 1e). First, the plate speeds up as the 410 km phase transition enhances the slab pull, then it slows down in response to the 660 km phase transition and to the viscosity increase in the lower mantle. In later stages, variations of plate velocity are driven by slab buckling (Čížková & Bina, 2013).

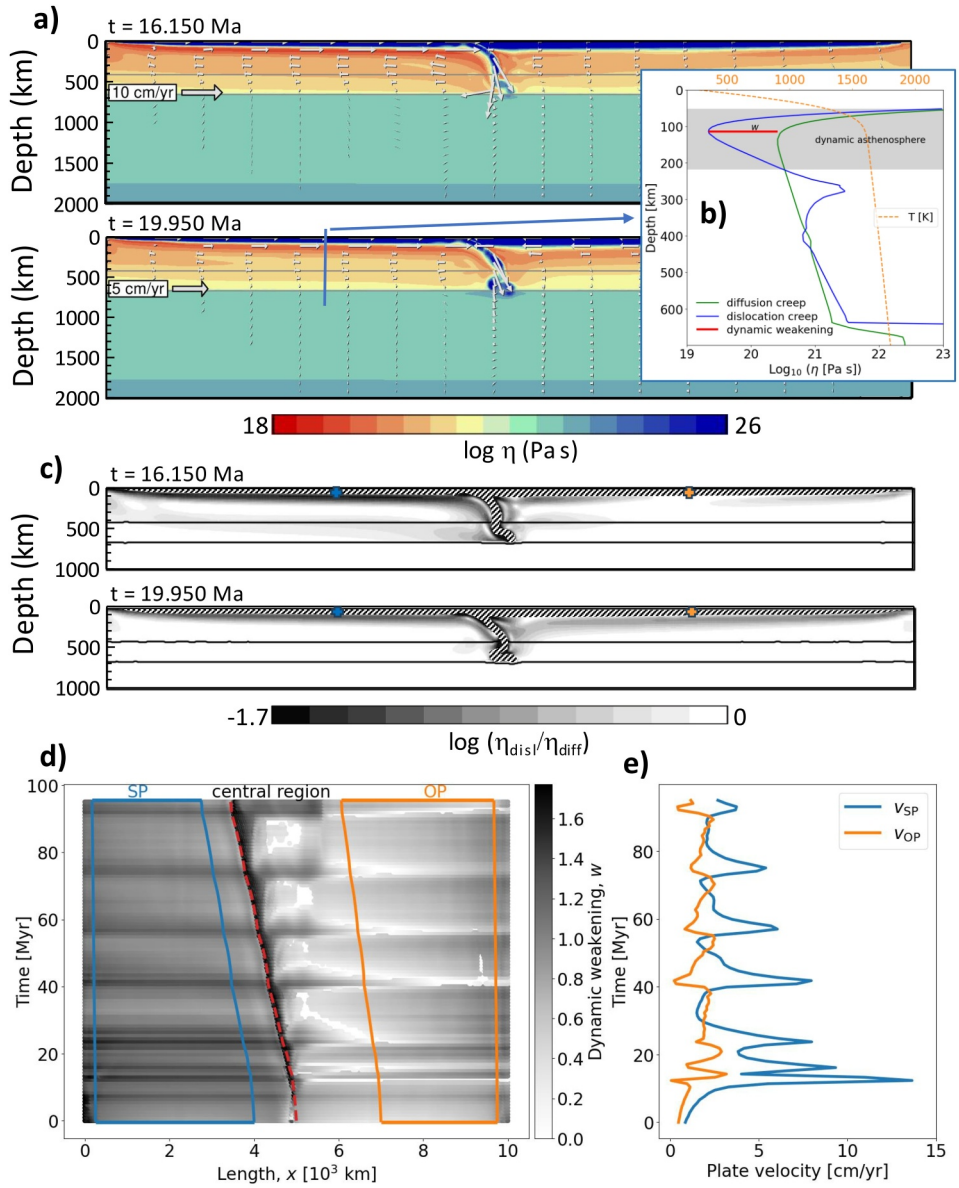

Figure 1. (a) Effective viscosity η_{eff} in model M4 (Table 1) for two snapshots in time (16.15 and 19.95 Myr). (b) Profile of diffusion and dislocation creep viscosity along a selected vertical line. Dynamic asthenosphere is marked in gray color, the amplitude of dynamic weakening w, Equation 5, is marked in red. Orange dashed line is the temperature profile. (c) Ratio of dislocation to diffusion creep viscosity in the upper mantle for the same snapshots as in panel (a) Blue and orange crosses depict tracers, placed inside the lithosphere, that are used to evaluate v_{SP} and v_{OP} respectively. Crosshatched regions mark the SP and OP. (d) Spatio-temporal evolution of dynamic weakening in model M4. Red dashed line marks the position of the trench, x_T, blue and orange lines indicate the length extent over which w is averaged to get $<w>$. (e) Temporal evolution of subducting (v_{SP}) and overriding (v_{OP}) plate velocities in the same model (M4).

We assume that the magnitude of strain-rate in the asthenosphere is primarily controlled by the contrast of plate velocity with respect to the underlying mantle and therefore aim to derive a relation between average dynamic weakening $<w>$ and the plate velocity v_P. Figure 2a shows that the plate velocity provides a primary control on the dynamic weakening below SP, because the same trend is observed for all performed models, that is, regardless of the initial plate age. Taking a simplistic approach, one can view the asthenosphere as a zone of thickness d where the velocity gradually changes from v_P to zero, giving the strain-rate $D = v_P/d$. Under additional simplifying assumptions that (a) the pressure and temperature at which the minimum dislocation creep viscosity is

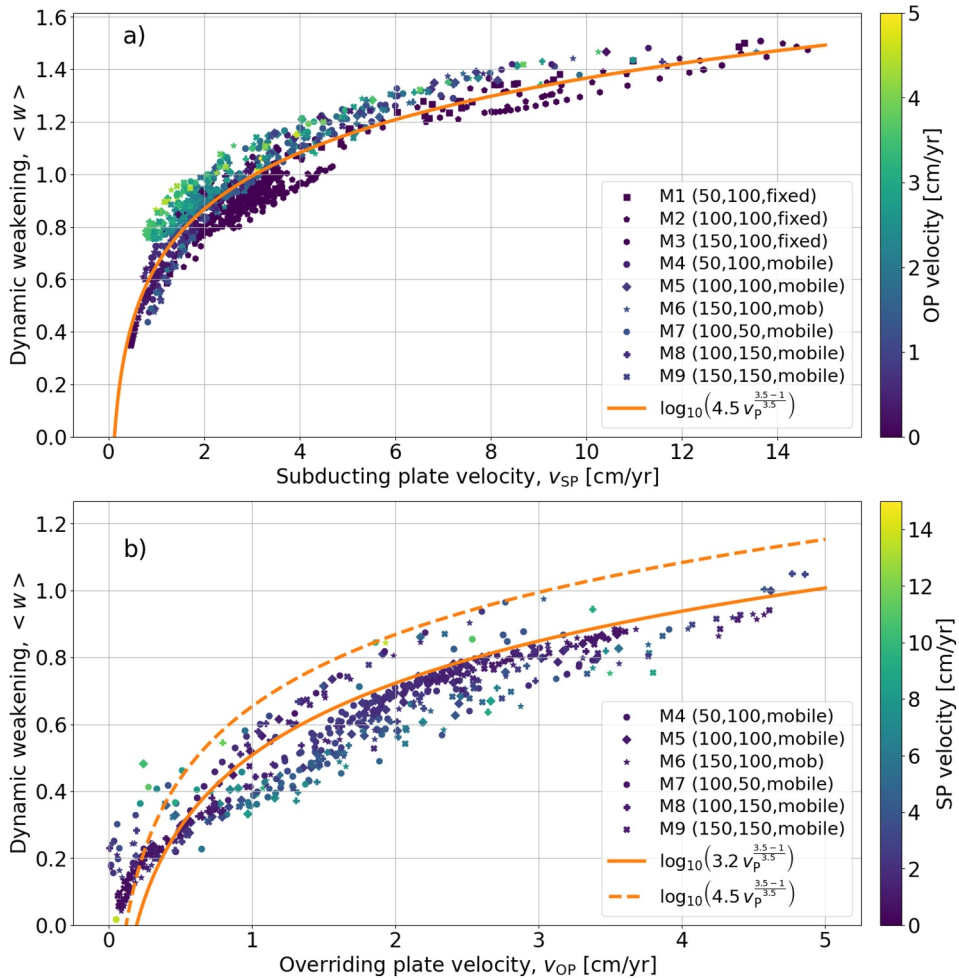

Figure 2. (a) Dynamic weakening w below the SP, averaged over the segment $x \in (0.05\, x_T, 0.8\, x_T)$ (cf. the blue segment in Figure 1d), plotted as a function of the SP velocity v_{SP}. Different symbols represent different models (Table 1), color marks the OP velocity v_{OP} in each respective snapshot in time. Orange curve shows the best fit of $<w>$ using Equation 6. (b) Dynamic weakening below the OP (orange segment in Figure 1d). Color marks the SP velocity, v_{SP}. Dashed line is the best fit solution from panel a, used later in Section 4.

reached, (b) the minimum diffusion creep viscosity, and (c) the thickness d are all constant, Equation 5 results in a logarithmic dependence of $<w>$ on v_P:

$$<w> = \log_{10}\left(C\, v_P^{\frac{n-1}{n}}\right) \tag{6}$$

where v_P is the plate velocity in cm/yr ($v_P = v_{SP}$ in Figure 2a and $v_P = v_{OP}$ in Figure 2b). Despite its simplicity, Equation 6, captures the obtained dynamic weakening reasonably well. Simultaneous fit of the data from all our simulations gives $C = 4.5$ below SP, with the root mean square error of the fit equal to 0.08.

In the family of fixed OP models, dynamic weakening is measured only below the SP. In mobile OP models, a similar effect is observed and measured also below the overriding plate. In Figure 2b, we plot $<w>$ evaluated below the OP as a function of the rollback velocity, v_{OP}. The weakening below OP is represented by an average value of w over the segment $(x - x_T)/(L - x_T) \in (0.4, 0.95)$, with $L = 10^4$ km denoting the model domain length (see the orange segment in Figure 1d).

Similarly to SP (Figure 2), also under OP the dependence of dynamic weakening on the plate velocity is comparable in all the investigated models, implying that the $<w>$ (v_P) scaling law, Equation 6, is applicable to a

generic subduction setting. The dynamic weakening is, however, less spatially uniform below OP when compared to SP (see Figure 1d), with w slightly increasing toward the right edge, making the average value $<w>$ somewhat dependent on the x-range over which the average is computed.

On average, the dynamic weakening below OP is slightly smaller than below SP ($C = 3.2$ vs. $C = 4.5$). This difference could be caused by the asthenosphere being thicker below the OP, or by the diffusion creep viscosity being smaller there. However, below both plates the dynamic asthenosphere has a similar average thickness, ca. 170 km, and a similar central depth of ca. 150 km. The most likely explanation of the difference in the C value is thus that the velocity contrast below SP is increased by the presence of a return flow (Figure 1a), making v_P/d only the lower estimate of the strain-rate below SP. Note that the central depth and thickness estimates agree with the common definition of asthenosphere that is based on seismic and electromagnetic sounding observations.

The color of symbols in Figure 2 marks the complementary plate velocity. Figure 2a shows that dynamic weakening below SP is enhanced when OP velocity is high, while dynamic weakening below OP seems to be slightly reduced for most data points with a high v_{SP}, with the exception of when the OP is nearly stagnant ($v_{OP} < 1$ cm/yr). This behavior is related to the interplay between the two plates during buckling, described below.

The SP velocity, v_{SP}, undergoes quasi-periodic variations (described in more detail in e.g. Čížková and Bina (2013)). In the episodes of fast v_{SP} when the dip angle of the slab increases, there is a negligible rollback and OP is more less stagnant. Below SP is a return flow whose strength, and thus the amplitude of dynamic weakening, is governed entirely by v_{SP} at this stage of subduction. Weakening of the mantle wedge is also dominated by v_{SP} during this stage, because the fast-sinking slab weakens the mantle at its base and above its upper surface. The overriding plate velocity, v_{OP} is typically small when v_{SP} is large, and dynamic weakening below OP is also small (Figure 1d).

In a complementary stage, typically when a large segment of the slab encounters an increased resistance at the 660 km phase transition, v_{SP} decreases and low dip angle results in a fast rollback episode accompanied by an increase of the rollback velocity (Figure 1e). The strength of return flow below SP is partly governed by how fast the SP is 'laying flat', which is, however, related to the rollback velocity, v_{OP}. This explains why the data points in Figure 2a that correspond to time steps with a high v_{OP} (bright color) show above average weakening. At this stage, v_{OP} is relatively large, and the mantle wedge is dominated by the flow below the OP, which has the same direction as that of the plate and magnitude decreasing with depth (Couette flow).

As a result, dynamic weakening above the already flat-lying slab shows a more complicated pattern and is cyclically governed by either v_{SP} or v_{OP}. This is a natural consequence of the fact that the central region (Figure 1d) progressively contains both plates, which disrupts the simple relation between asthenospheric viscosity and the surface plate velocity in Equation 6. We exclude the central region from the analysis in Figure 2.

Nevertheless, Equation 6 provides a reasonable first-order estimate for the global distribution of the dynamic weakening w. When the data sets from Figures 2a and 2b are combined and weighted such as to account for the uneven distribution of measurements along the x-axis, the best fit value of C is 4.5, that is, in the first decimal place it does not differ from the value obtained for SP in Figure 2a. In the next section, we thus apply the formula $w = \log_{10}\left(4.5\, v_P^{2.5/3.5}\right)$ to estimate the LVV below Earth's oceans.

4. Dynamic LVV

Inferring mantle viscosity from geophysical observations is a tedious but important task. The available data are insufficient to perform a 3D inversion without making additional simplifying assumptions (e.g., Čadek & Fleitout, 2003). One way to move forward is to improve our apriori knowledge of LVV in the mantle. In this section, we use the empirical law, Equation 6, to make a first-order estimate of LVV in the asthenosphere from reconstructed values of the absolute surface plate motions (Müller et al., 2019) (Figure 3).

Using Equation 6 globally is based on two simplifying assumptions. First, we assume that subduction dynamics dominates asthenospheric flow below the oceans. Coltice et al. (2019) evaluated the areal fraction F_D of the surface that is dragged by the interior in global mantle convection models with imposed continents. The average value of F_D was about 35% in their simulations, with the continental areas contributing to F_D proportionally more than the oceans. Their results imply that the surface plates are the main driver of the interior in oceanic regions,

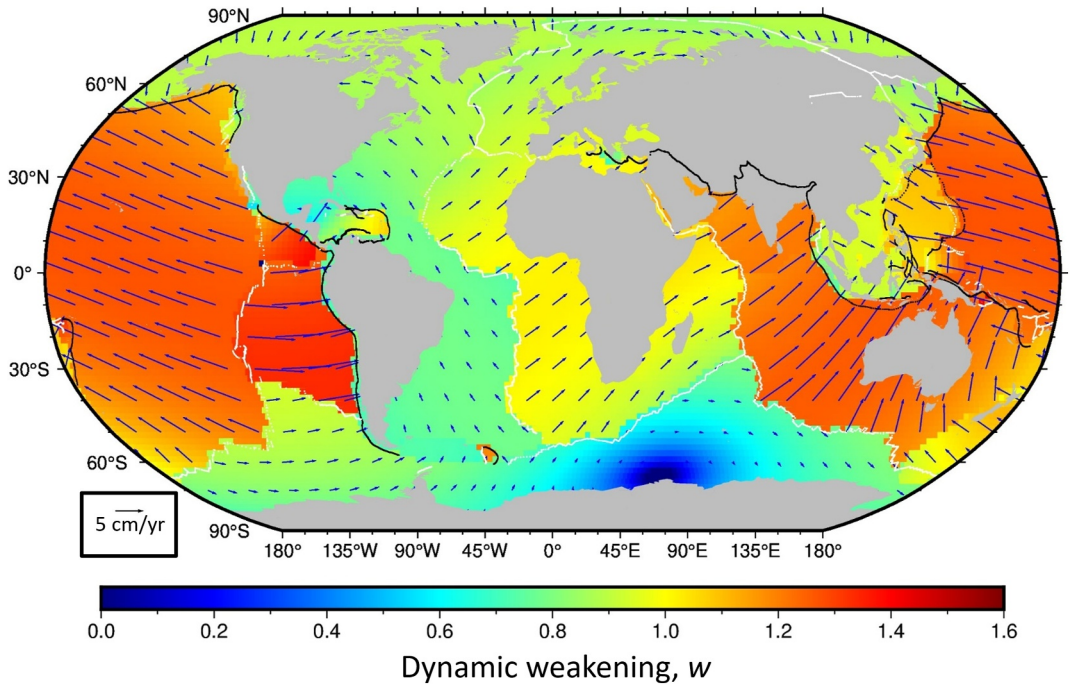

Figure 3. Dynamic weakening below Earth's oceanic plates. Vectors show the absolute plate velocities derived by Müller et al. (2019), obtained in a reference frame that minimizes net lithospheric rotation. Sublithospheric dynamic weakening, w, showed in color, is computed from these velocities using our empirical law, $w = \log_{10}\left(4.5\, v_P^{2.5/3.5}\right)$. The quantity w represents a first-order estimate of the lateral viscosity variations in the asthenosphere. Gray areas depict Earth's continents, black and white lines show the major trenches and ridges, respectively (Coffin, 1998).

consistently with our approach. Second, we apply Equation 6 to the entire area of oceanic plates, while the central and ridge regions were excluded from the analysis in Figure 2 (cf. Figure 1d).

Despite these crude simplifications, the dynamic LVV predicted in Figure 3 naturally explain several observations and help in resolving some problems experienced in previously published viscosity inversions. First of all, the dynamic weakening below the oceans is likely to be significantly larger than below the continents. While we restrict our analysis to oceans only, it can be expected that dynamic weakening below the continents is much smaller, because the drift of continents is on average much slower than the average velocity of oceanic plates (e.g., Torsvik et al., 2008). This result is in line with the findings of Ricard et al. (1991) and Čadek and Ricard (1992), who analyze the net rotation of the lithosphere (degree one toroidal velocities) and conclude that "asthenospheric viscosity below the oceans is at least one order of magnitude lower than underneath the continents", consistently with later geoid inversions (Čadek & Fleitout, 2003).

Secondly, the pacific plate is moving fast and thus is most lubricated. In order to match the present-day global surface velocities, Mao and Zhong (2021) had to reduce the resistance of the circum-pacific plate margin by a factor of ca. 7 with respect to other plate margins. However, if the asthenospheric LVV as predicted in Figure 3 were accounted for in their study, such an ad hoc reduction would not be necessary—the surface velocities of the pacific plate would increase even if the resistance of the circum-pacific plate margin was the same as the resistance of other plate margins. There are two dominant mechanisms that control the surface velocity of a plate: the resistance at its margin, and the friction at its base. The horizontal drag at the base of the pacific plate is significantly smaller than in most other regions (Figure 3), which may allow for its relatively large surface velocity without the circum-pacific margin's resistance being smaller when compared to other plate margins. Note also that the surface plate velocities by Müller et al. (2019) are computed such as to minimize the net lithospheric rotation—it is below 0.2°/Myr in their model. In reference frames that allow for faster net rotation rates, the westward velocities of plates increase (Doglioni et al., 2015). In this regard, the speed of the Pacific plate in Figure 3 is the bottom estimate.

Finally, the oldest and thus coldest slabs sink at the fastest rates. Our results therefore suggest that, at large wavelengths, the viscosity variations resulting from temperature effects should be partly compensated by the

dynamic weakening. This is in line with the fact that the inverted long-wavelength LVV (e.g., Yang & Gurnis, 2016) are much smaller than those predicted by forward models using laboratory-based constitutive relations for diffusion creep, in which the variations are suggested to be at least several orders of magnitude (e.g., Stadler et al., 2010).

Note that this study focuses on the oceanic plates and their velocity relative to the mantle. Becker (2006) has quantified the effect of power-law rheology on the viscosity variations in instantaneous global models of Earth mantle and has obtained oceanic asthenosphere weaker by ∼ one order of magnitude than the subcontinental regions, similarly to what we predict. In his study, however, the regional discrepancy of viscosity averages underneath oceanic and continental plates were reduced by the introduction of power-law flow. This is because strong continental roots were imposed in his models, and power-law creep dominated in the flow around them (cf. panels c and d of Figure 2 therein). While Becker (2006) concludes that models with LVV and power-law rheology show velocities that are similar to those of Newtonian, or purely radially-varying viscosity models, we argue that dislocation creep cannot not be neglected. Comparability of our simulations with previously published global geodynamic models and the role of numerical resolution is further discussed in the next section.

5. Discussion and Conclusions

We have evaluated the sublithospheric viscosity of dislocation and diffusion creep in a number of free subduction simulations. There is a significant dynamic weakening below both the subducting and the overriding plate, and it is primarily controlled by the amplitude of the surface velocity.

Given the importance of asthenosphere in the plate tectonics theory, our results warn against the use of numerical simulations with only diffusion creep. In a series of papers summarized by Lenardic et al. (2019), the viscosity contrast between the asthenosphere and the underlying mantle is linked with a sub-adiabatic temperature profile that results from an asymmetry between up- and down-wellings. Here, we show that a strong viscosity contrast may result simply from the relative motion of tectonic plates with respect to the underlying mantle.

The mutual feedback between plate velocities and their basal lubrication is likely to play a role during tectonic history of Earth. For present day plate velocities, the predicted dynamic weakening reaches up to 1.5 orders of magnitude (Figure 3). This value may be exceeded during episodes of rapid plate motion within the Wilson cycle, or locally in the mantle wedge region (Figure 1d, see also Billen and Hirth (2007) and Jadamec (2015)), but it generally stays within two orders of magnitude when plate velocities do not surpass a few tens of cm/yr.

The volume fraction of partial melt is likely less than 0.1% away from mid ocean ridges (e.g., S.-I. Karato, 2012), and the presence of the 150-km, that is, the first-stage melting boundary showed no correlation with radial seismic anisotropy, indicating that partial melt has no substantial effect on the large-scale viscosity of the asthenosphere (Hua et al., 2023).

When a 100–200 km thick asthenosphere is assumed, that is, consistently with the thickness obtained here, studies that invert for the viscosity profile from post-glacial rebound, post-seismic relaxation, as well as from the geoid, all suggest that the viscosity contrast between the asthenosphere and the underlying mantle is at least two orders of magnitude (for a summary and explanation of potential trade-offs, see M. A. Richards & Lenardic, 2018). Since the dynamically generated viscosity contrast is less than 10 below nearly half of the oceanic surface (Figure 3), additional weakening mechanisms must be present. Increased water content or elevated temperatures due to the accumulation of plume material are likely candidates, but assessing their relative importance is difficult, because the observational evidence is mostly indirect—perturbations of seismic velocities and electrical conductivity do not have a straightforward projection into the viscosity.

Based on post-seismic motion after three Chilean megathrust earthquakes, Boulze et al. (2022) have recently argued for a linear rheology in the asthenosphere, while others find post-seismic observations to be more consistent with a non-linear creep mechanism (e.g., Peña et al., 2020). Seemingly, the results presented here favor the latter interpretation, but it is important to point out the different settings of both experiments. Post-sesmic deformation is driven by short-term (a few years) stress relaxation near the subduction interface, and as such it reflects primarily the rheology of the subducted, hydrated crustal material rather than that of the suboceanic mantle investigated here. Moreover, the amplitude of the involved stresses as well as the time scales differ by orders of magnitude, which may result in the short-lived post-seismic deformation to appear Newtonian, although the long-term, plate tectonics driven background flow is facilitated by a non-linear asthenosphere (in a different

context, see Schmeling, 1987). Post-seismic inferences about asthenospheric rheology are therefore to be treated with care.

The presence or absence of asthenosphere is often debated in the context of Venus (e.g., Pauer et al., 2006). Recently, Maia et al. (2023) performed a global inversion of Venus's geoid and topography using a Bayesian inference approach. They inferred a ∼235 km thin, low-viscosity zone with a viscosity reduction of 5–15 times with respect to the underlying mantle. Given the different tectonic regime of Earth and Venus, a less pronounced asthenosphere on Venus is consistent with dynamic weakening being a significant, but not the sole mechanism involved.

There is a notable difference between the sublithospheric flow structure in our models when compared to typical global models (e.g., Coltice et al., 2019; Lenardic et al., 2019). While in the global models, Couette or Poiseuille flow dominates below the oceanic plates (i.e., plates drag the interior or the interior drags the surface plates), in our simulations, which contain more realistic slab dynamics, the sublithospheric mantle is driven by a return flow below the sinking slab (Figure 1a, the return flow is confined in the upper mantle). In this particular aspect, our simulations are similar to those presented by J. P. Morgan et al. (2013), who show that bulk of the asthenosphere resists being dragged down at the subduction zone (cf. their Figure 1 and Section 2.3). They argue that grid resolution of 4 km is needed to capture this behavior, far less than in typical global simulations. Note, however, that when slab penetrates into the lower mantle, which happens in models with fixed overriding plate, a whole-mantle convection cell develops below the SP. In our case, the return flow in the upper mantle is thus related to the folding of the slab in the transition zone rather than to the return of anomalously hot material as in J. P. Morgan et al. (2013). Data from all our models over the entire simulation time (100 Myr) are plotted in Figure 2a, indicating that the scaling law in Equation 6 captures the behavior both before and after the penetration of the slab into the lower mantle.

On the other hand, regional modeling suffers from the intrinsic incapability to capture how local dynamics affect the global flow structure, which in turn determines the boundary conditions of regional-scale models. To fully reconcile the above discrepancy, one must perform global numerical simulations with grid resolution of present-day regional models—a challenging task. In future work, global models with adaptive mesh refinement such as those by Stadler et al. (2010) could be used to quantify dynamic weakening below the continents as well as below the oceans. Note, however, that here we use self-consistently developed rather than seismically determined slab morphologies, which requires a significant number of computational time steps.

In one case or the other, strain rates are likely to be high below the fast moving tectonic plates, and we show that dynamic weakening due to dislocation creep is an important mechanism under such conditions, significantly contributing to the formation of the low-viscosity asthenosphere, with global variations related primarily to the different velocity of individual plates.

Data Availability Statement

The viscosity fields, interpolated onto a regular grid, and the time evolution of plate velocities in all models, as well as scripts that were used to produce Figures 1b–1e and 2 are available at Zenodo (Patočka, 2024). Figure 3 was produced using the python interface for the Generic Mapping Tool (pyGMT) software (https://www.pygmt.org/latest/).

Acknowledgments
We thank Arie van den Berg for discussions on the nonlinear rheology of upper mantle, Wim Spakman for sharing his script for viscosity/velocity plots, František Gallovič for discussions of post-seismic motions, and Ondřej Čadek for discussions on the viscosity differences below oceans and continents. We further thank Jeroen van Hunen and two anonymous reviewers for comments that helped to improve the manuscript, and Daoyuan Sun for his editorial work. This work has been supported by Charles University Research Centre program No. UNCE/24/SCI/005 and by the Czech Science Foundation through project No. 23-06345S.

References

Ahmed, O., & Lenardic, A. (2010). Low viscosity channels and the stability of long wavelength convection. *Physics of the Earth and Planetary Interiors*, *179*(3–4), 122–126. https://doi.org/10.1016/j.pepi.2010.01.008

Barrell, J. (1914). The strength of the earth's crust. *The Journal of Geology*, *22*(7), 655–683. https://doi.org/10.1086/622181

Becker, T. W. (2006). On the effect of temperature and strain-rate dependent viscosity on global mantle flow, net rotation, and plate-driving forces. *Geophysical Journal International*, *167*(2), 943–957. https://doi.org/10.1111/j.1365-246X.2006.03172.x

Becker, T. W., Conrad, C. P., Schaeffer, A. J., & Lebedev, S. (2014). Origin of azimuthal seismic anisotropy in oceanic plates and mantle. *Earth and Planetary Science Letters*, *401*, 236–250. https://doi.org/10.1016/j.epsl.2014.06.014

Bessat, A., Duretz, T., Hetényi, G., Pilet, S., & Schmalholz, S. M. (2020). Stress and deformation mechanisms at a subduction zone: Insights from 2-D thermomechanical numerical modelling. *Geophysical Journal International*, *221*(3), 1605–1625. https://doi.org/10.1093/gji/ggaa092

Billen, M., & Hirth, G. (2007). Rheologic controls on slab dynamics. *Geochemistry, Geophysics, Geosystems*, *8*(8), Q08012. https://doi.org/10.1029/2007GC001597

Bina, C. R., & Helffrich, G. (1994). Phase transition Clapeyron slopes and transition zone seismic discontinuity topography. *Journal of Geophysical Research*, *99*(B8), 15853–15860. https://doi.org/10.1029/94JB00462

Boulze, H., Fleitout, L., Klein, E., & Vigny, C. (2022). Post-seismic motion after 3 Chilean megathrust earthquakes: A clue for a linear asthenospheric viscosity. *Geophysical Journal International*, *231*(3), 1471–1478. https://doi.org/10.1093/gji/ggac255

Bunge, H., Richards, M., & Baumgardner, J. (1996). Effect of depth-dependent viscosity on the planform of mantle convection. *Nature*, *379*(6564), 436–438. https://doi.org/10.1038/379436a0

Busse, F., Richards, A., & Lenardic, A. (2006). A simple model of high Prandtl and high Rayleigh number convection bounded by thin low-viscosity layers. *Geophysical Journal International*, *164*(1), 160–167. https://doi.org/10.1111/j.1365-246X.2005.02836.x

Busse, F. H. (1985). Transition to turbulence in Rayleigh-Beénard convection. In H. L. Swinney & J. P. Gollub (Eds.), *Hydrodynamic instabilities and the transition to turbulence* (pp. 97–137). Springer Berlin Heidelberg. https://doi.org/10.1007/3-540-13319-4_15

Čadek, O., & Fleitout, L. (2003). Effect of lateral viscosity variations in the top 300 km on the geoid and dynamic topography. *Geophysical Journal International*, *152*(3), 566–580. https://doi.org/10.1046/j.1365-246X.2003.01859.x

Čadek, O., & Ricard, Y. (1992). Toroidal poloidal energy partitioning and global lithospheric rotation during Cenozoic time. *Earth and Planetary Science Letters*, *109*(3–4), 621–632. https://doi.org/10.1016/0012-821X(92)90120-K

Cammarano, F., Romanowicz, B., Stixrude, L., Lithgow-Bertelloni, C., & Xu, W. (2009). Inferring the thermochemical structure of the upper mantle from seismic data. *Geophysical Journal International*, *179*(2), 1169–1185. https://doi.org/10.1111/j.1365-246X.2009.04338.x

Carter, N., & Ave'Lallemant, H. (1970). High temperature flow of Dunite and Peridotite. *GSA Bulletin*, *81*(8), 2181–2202. https://doi.org/10.1130/0016-7606(1970)81[2181:HTFODA]2.0.CO;2

Cerpa, N. G., Sigloch, K., Garel, F., Heuret, A., Davies, D. R., & Mihalynuk, M. G. (2022). The effect of a weak asthenospheric layer on surface kinematics, subduction dynamics and slab morphology in the lower mantle. *Journal of Geophysical Research*, *127*(8), e2022JB024494. https://doi.org/10.1029/2022JB024494

Chertova, M., Geenen, T., van den Berg, A., & Spakman, W. (2012). Using open sidewalls for modelling self-consistent lithosphere subduction dynamics. *Solid Earth*, *3*(2), 313–326. https://doi.org/10.5194/se-3-313-2012

Čížková, H., & Bina, C. (2013). Effects of mantle and subduction-interface rheologies on slab stagnation and trench rollback. *Earth and Planetary Science Letters*, *379*, 95–103. https://doi.org/10.1016/j.epsl.2013.08.011

Čížková, H., van den Berg, A. P., Spakman, W., & Matyska, C. (2012). The viscosity of earth's lower mantle inferred from sinking speed of subducted lithosphere. *Physics of the Earth and Planetary Interiors*, *200*, 56–62. https://doi.org/10.1016/j.pepi.2012.02.010

Čížková, H., van Hunen, J., & van den Berg, A. (2007). Stress distribution within subducting slabs and their deformation in the transition zone. *Physics of the Earth and Planetary Interiors*, *161*(3–4), 202–214. https://doi.org/10.1016/j.pepi.2007.02.002

Coffin, M. (1998). Present-day plate boundary digital data compilation. *University of Texas Institute for geophysics technical report*, *174*, 5.

Coltice, N., Husson, L., Faccenna, C., & Arnould, M. (2019). What drives tectonic plates? *Science Advances*, *5*(10), eaax4295. https://doi.org/10.1126/sciadv.aax4295

Debayle, E., Kennett, B., & Priestley, K. (2005). Global azimuthal seismic anisotropy and the unique plate-motion deformation of Australia. *Nature*, *433*(7025), 509–512. https://doi.org/10.1038/nature03247

Doglioni, C., Carminati, E., Crespi, M., Cuffaro, M., Penati, M., & Riguzzi, F. (2015). Tectonically asymmetric earth: From net rotation to polarized westward drift of the lithosphere. *Geoscience Frontiers*, *6*(3), 401–418. https://doi.org/10.1016/j.gsf.2014.02.001

Dziewonski, A., & Anderson, D. (1981). Preliminary reference earth model. *Physics of the Earth and Planetary Interiors*, *25*(4), 297–356. https://doi.org/10.1016/0031-9201(81)90046-7

Forsyth, D., & Uyeda, S. (1975). Relative importance of driving forces of plate motion. *Geophysical Journal of the Royal Astronomical Society*, *43*(1), 163–200. https://doi.org/10.1111/j.1365-246X.1975.tb00631.x

Garel, F., Goes, S., Davies, D. R., Davies, J. H., Kramer, S. C., & Wilson, C. R. (2014). Interaction of subducted slabs with the mantle transition-zone: A regime diagram from 2-d thermo-mechanical models with a mobile trench and an overriding plate. *Geochemistry, Geophysics, Geosystems*, *15*(5), 1739–1765. https://doi.org/10.1002/2014GC005257

Green, H., & Radcliffe, S. (1972). Dislocation mechanisms in olivine and flow in the upper mantle. *Earth and Planetary Science Letters*, *15*(3), 239–247. https://doi.org/10.1016/0012-821X(72)90169-0

Hager, B., Clayton, R., Richards, M., Comer, R., & Dziewonski, A. (1985). Lower mantle heterogeneity, dynamic topography and the geoid. *Nature*, *313*(6003), 541–546. https://doi.org/10.1038/313541a0

Hager, B., & Richards, M. (1989). Long-wavelength variations in earth's geoid - Physical models and dynamical implications. *Philosophical Transactions of the Royal Society of London, Series A: Physical Sciences and Engineering*, *328*(1599), 309–327. https://doi.org/10.1098/rsta.1989.0038

Hirschmann, M. M. (2010). Partial melt in the oceanic low velocity zone. *Physics of the Earth and Planetary Interiors*, *179*(1–2), 60–71. https://doi.org/10.1016/j.pepi.2009.12.003

Hirth, G., & Kohlstedt, D. (2003). Rheology of the upper mantle and the mantle wedge: A view from the experimentalists. Inside the subduction factory. *Geophysical monograph*, *138*, 83–106. https://doi.org/10.1029/138GM06

Holt, A. F., & Becker, T. W. (2016). The effect of a power-law mantle viscosity on trench retreat rate. *Geophysical Journal International*, *208*(1), 491–507. https://doi.org/10.1093/gji/ggw392

Hua, J., Fischer, K. M., Becker, T. W., Gazel, E., & Hirth, G. (2023). Asthenospheric low-velocity zone consistent with globally prevalent partial melting. *Nature Geoscience*, *16*(2), 175–181. https://doi.org/10.1038/s41561-022-01116-9

Jadamec, M. A. (2015). Slab-driven mantle weakening and rapid mantle flow. In *Subduction dynamics* (pp. 135–155). American Geophysical Union (AGU). https://doi.org/10.1002/9781118888865.ch7

Jeanloz, R., & Morris, S. (1987). Is the mantle geotherm subadiabatic. *Geophysical Research Letters*, *14*(4), 335–338. https://doi.org/10.1029/GL014i004p00335

Kameyama, M., Yuen, D., & Karato, S. (1999). Thermal-mechanical effects of low-temperature plasticity (the Peierls mechanism) on the deformation of a viscoelastic shear zone. *Earth and Planetary Science Letters*, *168*(1–2), 159–172. https://doi.org/10.1016/s0012-821x(99)00040-0

Karato, S., & Wu, P. (1993). Rheology of the upper mantle—A synthesis. *Science*, *260*(5109), 771–778. https://doi.org/10.1126/science.260.5109.771

Karato, S.-I. (2008). Insights into the nature of plume-asthenosphere interaction from central pacific geophysical anomalies. *Earth and Planetary Science Letters*, *274*(1–2), 234–240. https://doi.org/10.1016/j.epsl.2008.07.033

Karato, S.-I. (2012). On the origin of the asthenosphere. *Earth and Planetary Science Letters*, *321*, 95–103. https://doi.org/10.1016/j.epsl.2012.01.001

Kawakatsu, H., Kumar, P., Takei, Y., Shinohara, M., Kanazawa, T., Araki, E., & Suyehiro, K. (2009). Seismic evidence for sharp lithosphere-asthenosphere boundaries of oceanic plates. *Science*, *324*(5926), 499–502. https://doi.org/10.1126/science.1169499

Lambert, I., & Wyllie, P. (1970). Low-velocity zone of earth's mantle - Incipient melting caused by water. *Science*, *169*(3947), 764–766. https://doi.org/10.1126/science.169.3947.764

Lenardic, A., Richards, M. A., & Busse, F. H. (2006). Depth-dependent rheology and the horizontal length scale of mantle convection. *Journal of Geophysical Research: Solid Earth*, *111*(B7), B07404. https://doi.org/10.1029/2005JB003639

Lenardic, A., Weller, M., Hoink, T., & Seales, J. (2019). Toward a boot strap hypothesis of plate tectonics: Feedbacks between plates, the asthenosphere, and the wavelength of mantle convection. *Physics of the Earth and Planetary Interiors*, *296*, 106299. https://doi.org/10.1016/j.pepi.2019.106299

Liu, H., Gurnis, M., & Leng, W. (2021). Constraints on mantle viscosity from slab dynamics. *Journal of Geophysical Research: Solid Earth*, *126*(8), e2021JB022329. https://doi.org/10.1029/2021JB022329

Maia, J. S., Wieczorek, M. A., & Plesa, A.-C. (2023). The mantle viscosity structure of Venus. *Geophysical Research Letters*, *50*(15), e2023GL103847. https://doi.org/10.1029/2023GL103847

Mallard, C., Coltice, N., Seton, M., Muller, R. D., & Tackley, P. J. (2016). Subduction controls the distribution and fragmentation of earth's tectonic plates. *Nature*, *535*(7610), 140+–143. https://doi.org/10.1038/nature17992

Mao, W., & Zhong, S. (2021). Constraints on mantle viscosity from intermediate-wavelength geoid anomalies in mantle convection models with plate motion history. *Journal of Geophysical Research: Solid Earth*, *126*(4), e2020JB021561. https://doi.org/10.1029/2020JB021561

Mierdel, K., Keppler, H., Smyth, J. R., & Langenhorst, F. (2007). Water solubility in aluminous orthopyroxene and the origin of earth's asthenosphere. *Science*, *315*(5810), 364–368. https://doi.org/10.1126/science.1135422

Mitrovica, J., & Forte, A. (2004). A new inference of mantle viscosity based upon joint inversion of convection and glacial isostatic adjustment data. *Earth and Planetary Science Letters*, *225*(1–2), 177–189. https://doi.org/10.1016/j.epsl.2004.06.005

Montagner, J., & Tanimoto, T. (1991). Global upper mantle tomography of seismic velocities and anisotropies. *Journal of Geophysical Research: Solid Earth*, *96*(B12), 20337–20351. https://doi.org/10.1029/91JB01890

Morgan, J., & Morgan, W. (1999). Two-stage melting and the geochemical evolution of the mantle: A recipe for mantle plum-pudding. *Earth and Planetary Science Letters*, *170*(3), 215–239. https://doi.org/10.1016/s0012-821x(99)00114-4

Morgan, J. P., Hasenclever, J., & Shi, C. (2013). New observational and experimental evidence for a plume-fed asthenosphere boundary layer in mantle convection. *Earth and Planetary Science Letters*, *366*, 99–111. https://doi.org/10.1016/j.epsl.2013.02.001

Müller, R. D., Zahirovic, S., Williams, S. E., Cannon, J., Seton, M., Bower, D. J., et al. (2019). A global plate model including lithospheric deformation along major rifts and orogens since the Triassic. *Tectonics*, *38*(6), 1884–1907. https://doi.org/10.1029/2018TC005462

Patočka, V. (2024). Simulation data for manuscript dynamic component of the asthenosphere: Lateral viscosity variations due to dislocation creep at the base of oceanic plates. *Zenodo*. https://doi.org/10.5281/zenodo.10499016

Pauer, M., Fleming, K., & Cadek, O. (2006). Modeling the dynamic component of the geoid and topography of Venus. *Journal of Geophysical Research*, *111*(E11), E11012. https://doi.org/10.1029/2005JE002511

Peltier, W. (1998). Postglacial variations in the level of the sea: Implications for climate dynamics and solid-earth geophysics. *Reviews of Geophysics*, *36*(4), 603–689. https://doi.org/10.1029/98RG02638

Peña, C., Heidbach, O., Moreno, M., Bedford, J., Ziegler, M., Tassara, A., & Oncken, O. (2020). Impact of power-law rheology on the viscoelastic relaxation pattern and afterslip distribution following the 2010 mw 8.8 Maule earthquake. *Earth and Planetary Science Letters*, *542*, 116292. https://doi.org/10.1016/j.epsl.2020.116292

Pokorný, J., Čížková, H., Bina, C., & van den Berg, A. (2023). 2d stress rotation in the Tonga subduction region. *Earth and Planetary Science Letters*, *621*, 118379. https://doi.org/10.1016/j.epsl.2023.118379

Pokorný, J., Čížková, H., & van den Berg, A. (2021). Feedbacks between subduction dynamics and slab deformation: Combined effects of nonlinear rheology of a weak decoupling layer and phase transitions. *Physics of the Earth and Planetary Interiors*, *313*, 106679. https://doi.org/10.1016/j.pepi.2021.106679

Ricard, Y., Doglioni, C., & Sabadini, R. (1991). Differential rotation between lithosphere and mantle—A consequence of lateral mantle viscosity variations. *Journal of Geophysical Research*, *96*(B5), 8407–8415. https://doi.org/10.1029/91JB00204

Ricard, Y., Richards, M., Lithgow-Bertelloni, C., & Lestunff, Y. (1993). A geodynamic model of mantle density heterogeneity. *J. Geophys. Res. Solid Earth*, *98*(B12), 21895–21909. https://doi.org/10.1029/93JB02216

Richards, M., & Engebretson, D. (1992). Large-scale mantle convection and the history of subduction. *Nature*, *355*(6359), 437–440. https://doi.org/10.1038/355437a0

Richards, M. A., & Lenardic, A. (2018). The cathles parameter (ct): A geodynamic definition of the asthenosphere and implications for the nature of plate tectonics. *Geochemistry, Geophysics, Geosystems*, *19*(12), 4858–4875. https://doi.org/10.1029/2018GC007664

Rychert, C. A., & Shearer, P. M. (2009). A global view of the lithosphere-asthenosphere boundary. *Science*, *324*(5926), 495–498. https://doi.org/10.1126/science.1169754

Schmeling, H. (1987). On the interaction between small- and large-scale convection and postglacial rebound flow in a power-law mantle. *Earth and Planetary Science Letters*, *84*(2), 254–262. https://doi.org/10.1016/0012-821X(87)90090-2

Schulz, F., Tosi, N., Plesa, A.-C., & Breuer, D. (2020). Stagnant-lid convection with diffusion and dislocation creep rheology: Influence of a non-evolving grain size. *Geophysical Journal International*, *220*(1), 18–36. https://doi.org/10.1093/gji/ggz417

Segal, A., & Praagman, N. (2005). The SEPRAN FEM package. Technical report. *Ingenieursbureau SEPRA*. http://ta.twi.tudelft.nl/sepran/sepran.html

Semple, A., & Lenardic, A. (2020). The robustness of pressure-driven asthenospheric flow in mantle convection models with plate-like behavior. *Geophysical Research Letters*, *47*(17), e2020GL089556. https://doi.org/10.1029/2020GL089556

Semple, A. G., & Lenardic, A. (2018). Plug flow in the earth's asthenosphere. *Earth and Planetary Science Letters*, *496*, 29–36. https://doi.org/10.1016/j.epsl.2018.05.030

Semple, A. G., & Lenardic, A. (2021). Feedbacks between a non-Newtonian upper mantle, mantle viscosity structure and mantle dynamics. *Geophysical Journal International*, *224*(2), 961–972. https://doi.org/10.1093/gji/ggaa495

Shankland, T., O'Connell, R., & Waff, H. (1981). Geophysical constraints on partial melt in the upper mantle. *Reviews of Geophysics*, *19*(3), 394–406. https://doi.org/10.1029/RG019i003p00394

Stadler, G., Gurnis, M., Burstedde, C., Wilcox, L. C., Alisic, L., & Ghattas, O. (2010). The dynamics of plate tectonics and mantle flow: From local to global scales. *Science*, *329*(5995), 1033–1038. https://doi.org/10.1126/science.1191223

Steinbach, V., & Yuen, D. A. (1995). The effects of temperature-dependent viscosity on mantle convection with the two major phase transitions. *Physics of the Earth and Planetary Interiors*, *90*(1), 13–36. https://doi.org/10.1016/0031-9201(95)03018-R

Su, W., & Dziewonski, A. (1992). On the scale of mantle heterogeneity. *Physics of the Earth and Planetary Interiors*, *74*(1–2), 29–54. https://doi.org/10.1016/0031-9201(92)90066-5

Torsvik, T. H., Müller, R. D., Van der Voo, R., Steinberger, B., & Gaina, C. (2008). Global plate motion frames: Toward a unified model. *Reviews of Geophysics*, *46*(3), RG3004. https://doi.org/10.1029/2007RG000227

Turcotte, D. L., & Schubert, G. (1982). Geodynamics. In *Geodynamics* (pp. 134–159). John Wiley and Sons.

van den Berg, A., van Keken, P., & Yuen, D. (1993). The effects of a composite non-Newtonian and Newtonian rheology on mantle convection. *Geophysical Journal International*, *115*(1), 62–78. https://doi.org/10.1111/j.1365-246x.1993.tb05588.x

van Hunen, J., Zhong, S., Shapiro, N. M., & Ritzwoller, M. H. (2005). New evidence for dislocation creep from 3-d geodynamic modeling of the pacific upper mantle structure. *Earth and Planetary Science Letters*, *238*(1–2), 146–155. https://doi.org/10.1016/j.epsl.2005.07.006

Walpole, J., Wookey, J., Kendall, J.-M., & Masters, T.-G. (2017). Seismic anisotropy and mantle flow below subducting slabs. *Earth and Planetary Science Letters*, *465*, 155–167. https://doi.org/10.1016/j.epsl.2017.02.023

Yang, T., & Gurnis, M. (2016). Dynamic topography, gravity and the role of lateral viscosity variations from inversion of global mantle flow. *Geophysical Journal International*, *207*(2), 1186–1202. https://doi.org/10.1093/gji/ggw335

Yang, T., Moresi, L., Zhao, D., Sandiford, D., & Whittaker, J. (2018). Cenozoic lithospheric deformation in northeast Asia and the rapidly-aging Pacific plate. *Earth and Planetary Science Letters*, *492*, 1–11. https://doi.org/10.1016/j.epsl.2018.03.057